An Angular Stabilized Frequency Selective Surface by Using Capacitance Layers Structure

Meng Sun[1], Shaowei Bie[1, *], Ling Miao[1], Qian Chen[2], and Jianjun Jiang[1]

Abstract—A band-pass frequency selective surface (FSS) structure using capacitance layers is proposed to improve the performance of angular stability. It consists of band-pass FSSs, supporting dielectrics, and capacitance layers out of band-pass FSS. The supporting dielectrics and capacitance layers work as a transmission line and capacitance impedance matcher. Through the impedance matcher, the bandwidth is stabilized, and insertion loss at passband is reduced from -0.76 dB to -0.39 dB for incident angles up to $60°$. The equivalent circuit of the proposed structure is presented, and the Smith chart is given to explain the mechanism of the capacitance layers. Finally, a prototype is manufactured and measured. A relatively good agreement is obtained between simulations and measurements. Therefore, the proposed structure can be an effective solution to improve the angular stability performance of band-pass FSS design.

1. INTRODUCTION

Typical frequency selective surfaces are one- or two-dimensional periodic structures which consist of metal patterns and dielectric substrates. FSS is essentially a kind of spatial filter, which does not absorb any energy itself. In recent years, FSS has been drawing a lot of attention for working as a spatial filter with a band-pass characteristics [1–10]. They are widely used in the electromagnetic field as filters, absorbers, radomes, and antenna reflectors. However, the properties of resonant frequency, bandwidth, and insertion loss are different from normal incidence for a band-pass FSS when the incident angle changes. Thus, the problem of angular stability becomes a major concern for actual applications.

The common techniques to improve angular stability can be classified into two categories. In the first category, miniaturized elements frequency surface (MEFSS) is utilized to improve the oblique incident performance through reducing the unit size. Parker et al. have proposed a method in which the metal lines were twisted and turned to increase the electrical length and reduce the unit size, and went a step further, interwoven elements were proposed, in which the coupling effect between neighbor elements was enhanced to make the unit size smaller [1, 2, 9, 10]. Then another method has been proposed by Liu et al. that metal patterns can be replaced by capacitors (C) or inductors (L). The unit size was greatly reduced, and the resonant frequency mainly depended on the value of C and L [3]. In recent years, Sarabandi and Behdad have proposed a new miniaturized structure [4–7, 11], which used strong coupling between the capacitive layer and inductive layer to realize miniaturized unit. MEFSS can make the imaginary part of FSS's impedance stable, so the performance of resonant frequency was improved. In order to improve the performance of bandwidth, that is, stabilizing the real part of impedance, the second category outer dielectric bonding technique is required. Loading dielectrics with relative permittivity of $1 + \cos\theta$ (θ is the maximum of incident angle) at both sides of FSS is an effective way to get a constant bandwidth and flat top [7, 8, 12] according to Munk.

In this letter, the authors propose a band-pass structure by using capacitance layers to reduce the insertion loss and stabilize the resonant frequency and bandwidth over a wide angular-range. The structure consists of a second-order band-pass FSS structure, supporting dielectrics and capacitive FSSs. Simulations by HFSS are completed. Results show that the performance is better in insertion loss, resonant frequency, and bandwidth under the capacitance layers structure than the individual band-pass FSS structure. To verify the simulation results, a prototype is fabricated and measured. The results of measurement are consistent with simulations.

2. ANGULAR STABILIZED BAND-PASS FILTER AND ITS PERFORMANCES

2.1. Band-Pass Structure

According to the existing methods, planar-type band-pass FSS can be achieved by slot FSS or combination of inductive grid FSS and capacitive patches FSS. Normally, slot FSS has a more stable performance in resonant frequency since the FSSs combination is sensitive to the thickness of dielectrics between FSSs. In addition, because of the shape and triangle configuration, the hexagon loop slot has smaller element size than other simple patterns like square loop slot and ring slot. Therefore, the second order band-pass structure is designed with a unit cell of hexagon loop slot and configuration of are gular triangle. The structure is shown in Figure 1, and pertinent geometric parameters of the structure are defined as follows: $h_1 = 7\,\text{mm}$, $p = 10\,\text{mm}$, $r = 3.8\,\text{mm}$, $s = 1.5\,\text{mm}$. It is generally known that metallic lines can be equivalent to an inductor (L), and slots can be equivalent to a capacitor (C) under the incident electromagnetic wave, so the second order band-pass structure can be equivalent to a L-C parallel circuit which is shown in Figure 1, and the resonance frequency is determined by L and C.
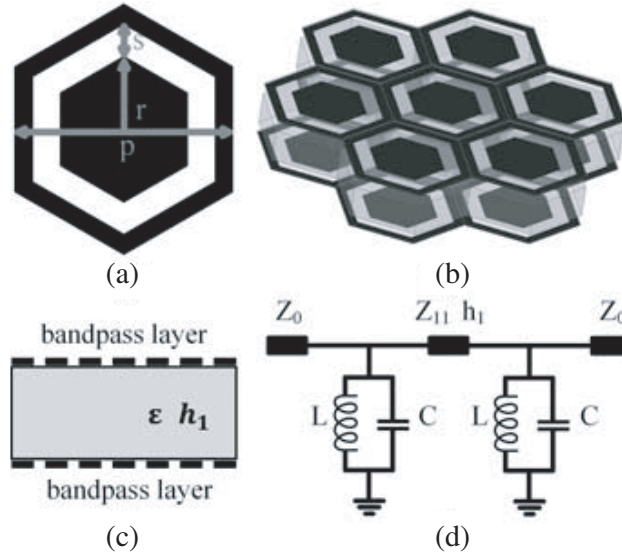

Figure 1. Configuration of the band-pass structure. (a) Top view of the unit cell. (b) 3-D view. (c) Side view. (d) Equivalent circuit.

Table 1. Performance parameters of band-pass structure.

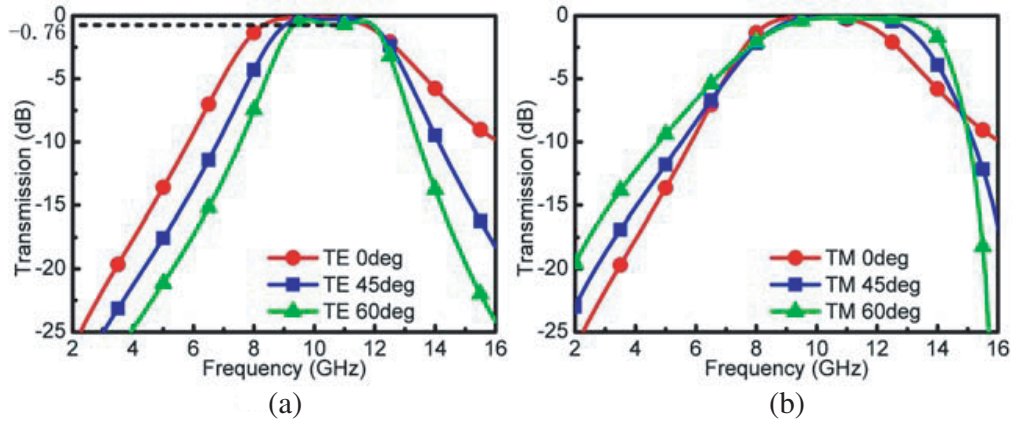|	f_L ($-3\,$dB)	f_H ($-3\,$dB)	Center Frequency	Bandwidth
0° (TE)	7.4 GHz	13 GHz	10.2 GHz	5.6 GHz
60° (TE)	8.7 GHz	12.5 GHz	10.6 GHz	4.1 GHz
0° (TM)	7.4 GHz	12.9 GHz	10.15 GHz	5.5 GHz
60° (TM)	7.5 GHz	14.3 GHz	10.9 GHz	6.8 GHz

Figure 2. Simulated transmission coefficient of the band-pass structure.

Simulations by HFSS are completed. The transmission coefficient of the structure is shown in Figure 2, and its corresponding parameters is shown in Table 1. The insertion loss at normal incidence is higher than oblique incidence, especially in TE mode. The resonant frequency moves to higher values, and bandwidth is reduced in TE mode and increased in TM mode.

2.2. Band-Pass Structure with Capacitance Layers

In order to improve the angular stability, capacitance layer structures are added on both sides of the second order band-pass structure. The four-tier structure of angular stabilized band-pass filter is shown in Figure 3 in which black areas represent metallic lines. The geometric parameters of the FSS are defined as follows: $h_0 = 5\,\text{mm}$, $h_1 = 7\,\text{mm}$, $p = 10\,\text{mm}$, $r = 3.8\,\text{mm}$, $s = 1.5\,\text{mm}$, $a = 2.2\,\text{mm}$, $b = 1\,\text{mm}$. Dielectric support between capacitance layer and band-pass layer are honeycomb with
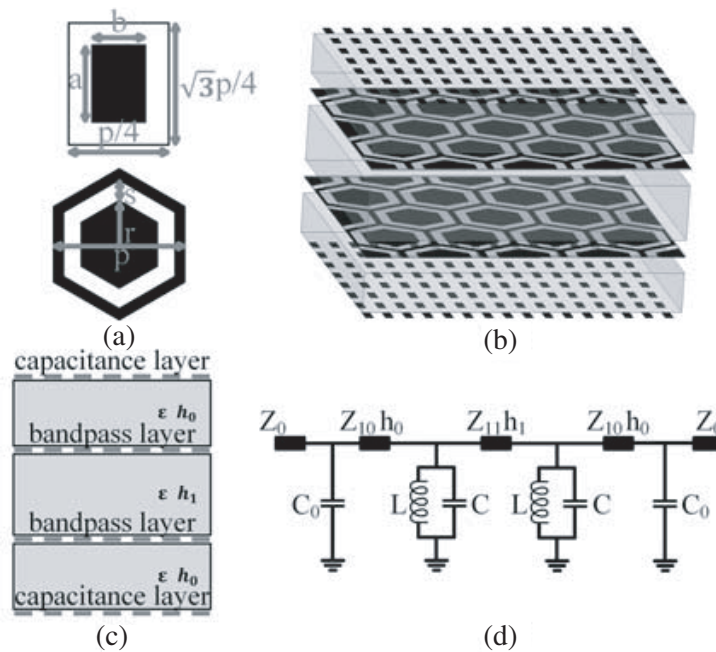

Figure 3. Configuration of the angular stabilized band-pass structure. (a) Top view of the unit cell. (b) 3-D view. (c) Side view. (d) Equivalent circuit.

relative permittivity of $\varepsilon_1 = 1.07$. Its equivalent circuit is shown in Figure 3(d). The capacitance layers are equivalent to a capacitor (C_0) approximately because the value of equivalent inductance is so small to be ignored compared to the equivalent capacitance. Support honeycomb between FSSs can be equivalent to lossless transmission lines Z_{10} and Z_{11}. Therefore, the lossless transmission line Z_{10} and capacitor C_0 produce a transmission line-capacitance (T-C) matching network which can improve the performance of angular stability according to the impedance matching theory. Thickness of the honeycomb and the rectangle size of capacitance FSS are adjustable so as to realize impedance matching for different cases.

To verify the stabilized performance of the structure, simulations of the band-pass FSS with capacitance layers is completed by HFSS. As shown in Figure 4 and Table 2, the insertion loss at 60° is reduced from -0.76 dB to -0.39 dB, and the bandwidth of TM mode also has a better performance than normal incidence. Bandwidth of -3 dB is 7.4 GHz–14 GHz, and for 60° incidence, bandwidth is 7.3 GHz–14.5 GHz. In addition, the center frequency of passband is more stable especially for TM mode.
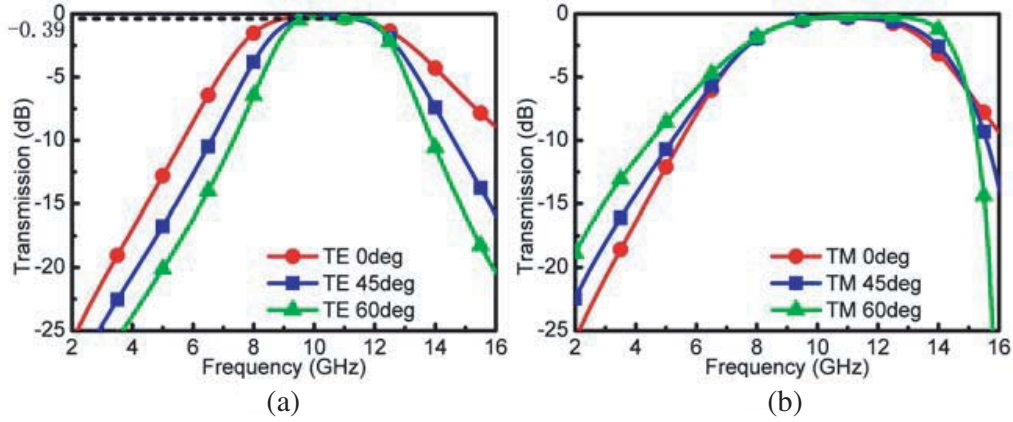

Figure 4. Simulated transmission coefficient of the band-pass structure with capacitance layers.

Table 2. Performance parameters of band-pass structure with T-C matching network.

	f_L (-3 dB)	f_H (-3 dB)	Center Frequency	Bandwidth
0° (TE)	7.4 GHz	13.5 GHz	10.45 GHz	6.1 GHz
60° (TE)	8.6 GHz	12.7 GHz	10.65 GHz	4.1 GHz
0° (TM)	7.4 GHz	14 GHz	10.7 GHz	6.6 GHz
60° (TM)	7.3 GHz	14.6 GHz	11.95 GHz	7.3 GHz

2.3. Mechanism Analysis

To explain the mechanism, Smith chart of reflection coefficients of the structure is given in Figure 5. Line 1 is for band-pass (BP) layers only. According to the transmission line theory, the free space impedance changes from $Z_0(120\pi)$ for both TE and TM modes to $Z_0/\cos\theta$ for TE mode and $Z_0 \times \cos\theta$ for TM mode when the incident angle changes from 0 to θ, and the thickness of the dielectric support also changes from h_1 to $h_1 \times \cos\theta$. Therefore, compared to the normal incidence, the resonant frequency shifts to a higher frequency; insertion loss is increased; bandwidth is reduced for TE mode; the resonant frequency shifts to a higher frequency; insertion loss is stable; and bandwidth is increased for the TM mode. Then, line 2 is for the band-pass structure after adding the honeycomb at both sides of the band-pass layers. For the honeycomb transmission line (TL), the points on line 1 rotate along the constant resistance circle to line 2, and the phase is changed, but the amplitude is basically unchanged. So, compared to line 1, curves in Figure 5 of line 2 are different from curves of line 1, but the transmission coefficient of band-pass structure with TL is almost consistent with the transmission coefficient of band-pass structure only. According to the principle of impedance matching, there is a note that the thickness
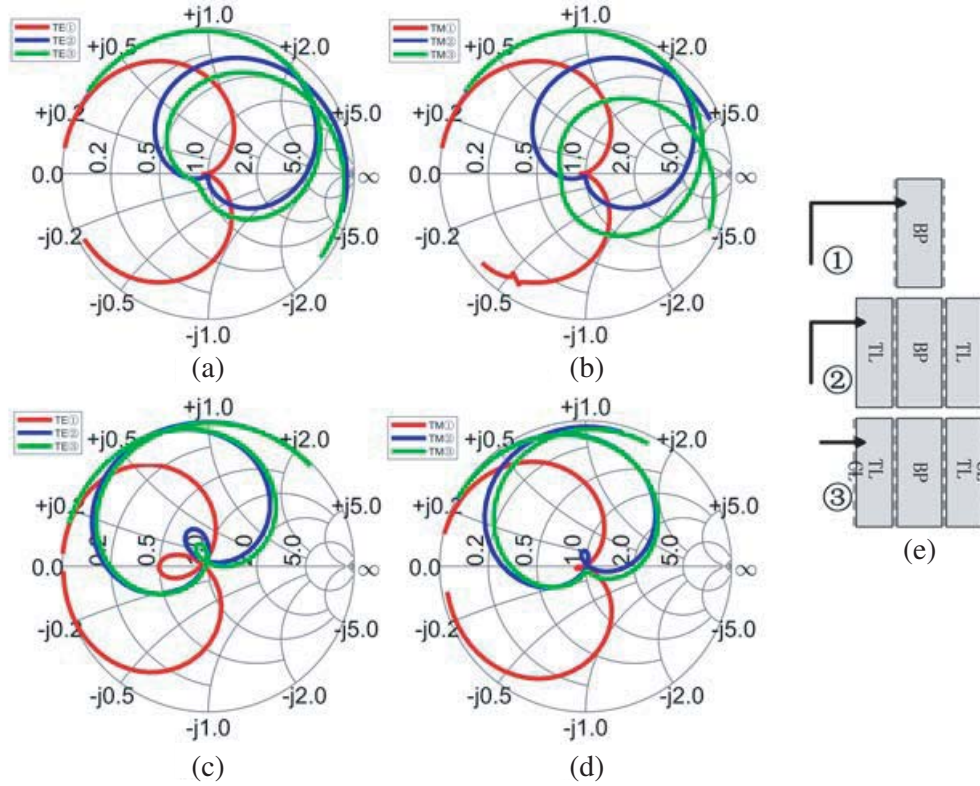
Figure 5. Smith chart of the stabilization process from 2–16 GHz. (a) 0°, TE mode. (b) 0°, TM mode. (c) 60°, TE mode. (d) 60°, TM mode. (e) Structure diagram.

h_0 is designed to satisfy the condition for $2\beta h_0 \times \cos\theta < \pi/2$ to reduce the insertion loss at 60°, so h_0 is slightly smaller than $\lambda/4$ where λ refers to the wave length of the resonant frequency. Finally, after adding the capacitance layers (CL), points on line 2 rotate along the constant conductivity circle to line 3. For the capacitance layers and transmission line, the effects on normal incidence and oblique incidence are different. For normal incidence, both TE and TM modes have a lower reflection coefficient on the low frequency side and higher reflection coefficient on the high frequency side which means that the resonant frequency is shifted to a higher value. For oblique incidence, for example 60°, both TE and TM modes have a lower reflection coefficient on the low frequency side, but the reflection coefficient on the high frequency side changes little since the curve is near the real axis on the high frequency side. Therefore, bandwidth is reduced. Thus, through a reasonable design, performance of resonant frequency and bandwidth can be improved. In addition, as shown in Figure 3(c), the maximum insertion loss points at passband of line 2 are in the fourth quadrant since h_0 is slightly smaller than $\lambda/4$, thus the insertion loss is reduced by the effect of capacitance layers.

3. FABRICATION AND MEASUREMENT

To experimentally demonstrate the performance of transmission for oblique incidence, a prototype of the proposed FSS is fabricated using wet etching and measured using a free-space measurement setup. Band-pass FSS is fabricated on FR4 substrates with $\varepsilon_r = 4.4$ and thickness 0.15 mm, and capacitance FSS is fabricated on PI films with $\varepsilon_r = 3.4$ and thickness 0.025 mm. In addition, Honeycomb is used as a support between FSSs with $\varepsilon_r = 1.07$. The thickness of honeycomb is adjustable for different resonant frequencies and incident angles. The dimension of the band-pass FSSs and capacitance FSSs samples is 300×300 mm^2. The measurement setup consists of a transmitting horn antenna, a receiving horn antenna, absorption screens, and an Agilent 8720ES vector network analyzer, as shown in Figure 6. The measured transmission performances of both TE and TM modes at 0°, 45°, and 60° of the structure
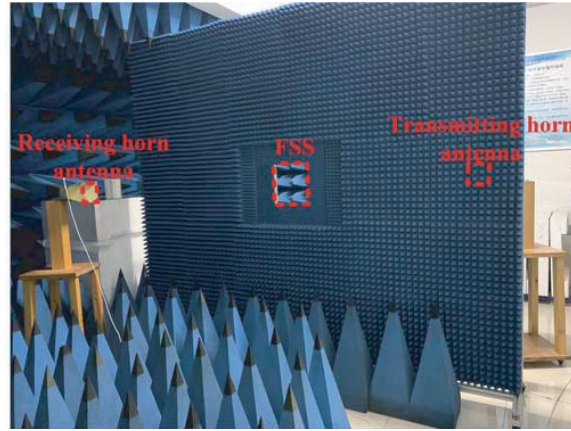
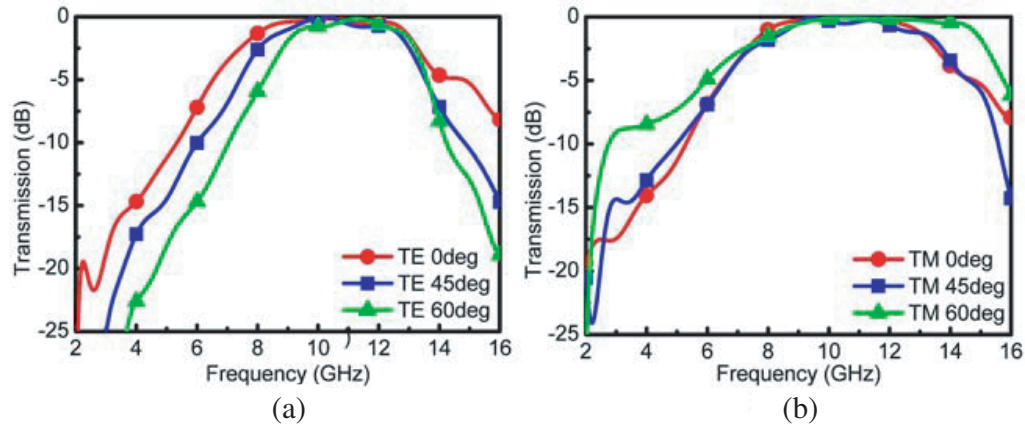**Figure 6.** Test environment of transmission coefficient.

Figure 7. Measured transmission coefficients of the angular stabilized band-pass FSS for different polarizations and incident angles. (a) TE mode. (b) TM mode.

are shown in Figure 7. The measured results of resonant frequency and bandwidth basically tally with the simulated results.

4. CONCLUSION

In this letter, an angular stabilized second order band-pass FSS using a capacitance layers structure is proposed. An AT-C matching network is introduced to improve its angular stability as the incident angle changes from normal to $60°$. Moreover, the mechanism is analyzed by equivalent circuit and Smith chart. Finally, the structure is fabricated and measured. The results show that the performance of angular stability is improved for resonant frequency, bandwidth, and insertion loss. The experimental results agree with the simulated ones.

ACKNOWLEDGMENT

REFERENCES

1. Zhao, P., Z. Zong, W. Wu, B. Li, and D. Fang, "Miniaturized-element bandpass FSS by loading capacitive structures," *IEEE Transactions on Antennas and Propagation*, Vol. 67, No. 5, 3539–3544, May 2019.

2. Li, D., Z. Shen, and E. P. Li, "Spurious-free dual-band bandpass frequency-selective surfaces with large band ratio," *IEEE Transactions on Antennas and Propagation*, Vol. 67, No. 2, 1065–1072, Feb. 2019.

3. Liu, H. L., K. L. Ford, and R. J. Langley, "Design methodology for a miniaturized frequency selective surface using lumped reactive components," *IEEE Transactions on Antennas and Propagation*, Vol. 57, No. 9, 2732–2738, Sep. 2009.

4. Sarabandi, K. and N. Behdad, "A frequency selective surface with miniaturized elements," *IEEE Transactions on Antennas and Propagation*, Vol. 55, No. 5, 1239–1245, May 2007.

5. Li, T. W., D. Li, and E. P. Li, "A novel FSS structure with high selectivity and excellent angular stability for 5G communication radome," *2017 10th Global Symposium on Millimeter-Waves*, 50–52, Hong Kong, 2017.

6. Wang, H., L. Zheng, M. Yan, J. Wang, S. Qu, and R. Luo, "Design and analysis of miniaturized low profile and second-order multi-band polarization selective surface for multipath communication application," *IEEE Access*, Vol. 7, 13455–13467, 2019.

7. Liu, X., Q. Wang, W. Zhang, M. Jin, and M. Bai, "On the improvement of angular stability of the 2nd-order miniaturized FSS structure," *IEEE Antennas and Wireless Propagation Letters*, Vol. 15, 826–829, 2016.

8. Liang, E. and T. K. Wu, "Novel wideband frequency selective surface filters with fractal elements," *Microwave Journal*, Vol. 60, 102–110, Nov. 2017.

9. Parker, E. A., A. N. A. El Sheikh, C. De, and A. C. Lima, "Convoluted frequency-selective array elements derived from linear and crossed dipoles," *IEE Proc. H*, Vol. 140, No. 5, 378–380, 1993.

10. Yan, M., S. Qu, H. Ma, et al., "Convoluted element frequency selective surface with miniaturization and wideband response," *2016 IEEE MTT-S International Microwave Workshop Series on Advanced Materials and Processes for RF and THz Applications (IMWS-AMP)*, 1–3, Chengdu, 2016.

11. Omar, A. A. and Z. Shen, "Thin bandstop frequency-selective structures based on loop resonator," *IEEE Transactions on Microwave Theory and Techniques*, Vol. 65, No. 7, 2298–2309, Jul. 2017.

12. Munk, B., *Frequency Selective Surfaces: Theory and Design*, Wiley, New York, NY, USA, 2000.